J. metamorphic Geol., 2002, **20,** 669–682

Successive hydration and dehydration of high-*P* mafic granofels involving clinopyroxene–kyanite symplectites, Mt Daniel, Fiordland, New Zealand

N. R. DACZKO[1,*], J. A. STEVENSON[1], G. L. CLARKE[1] AND K. A. KLEPEIS[2]
[1]*School of Geosciences, FO5, University of Sydney, Sydney, NSW 2006, Australia (geoffc@mail.usyd.edu.au)*
[2]*Department of Geology, University of Vermont, Burlington, VT 05405, USA*

ABSTRACT Three texturally distinct symplectites occur in mafic granofels of the Arthur River Complex at Mt Daniel, Fiordland, New Zealand. These include symplectic intergrowths of clinopyroxene and kyanite, described here for the first time. Pods of mafic granofels occur within the contact aureole of the Early Cretaceous Western Fiordland Orthogneiss batholith. The pods have cores formed entirely of garnet and clinopyroxene, and rims of pseudomorphous coarse-grained symplectic intergrowths of hornblende and clinozoisite that reflect hydration at moderate to high-*P*. These hornfelsic rocks are enveloped by a hornblende–clinozoisite gneissic foliation (S1). Narrow garnet reaction zones, in which hornblende and clinozoisite are replaced by garnet–clinopyroxene assemblages, developed adjacent to fractures and veins that cut S1. Fine-grained symplectic intergrowths of (1) clinopyroxene and kyanite and (2) clinozoisite, quartz, kyanite and plagioclase form part of the garnet reaction zones and partially replace coarse-grained S1 hornblende and clinozoisite. The development of the garnet reaction zones and symplectites was promoted by dehydration most probably following cooling of the contact aureole. Maps of oxide weight percent and cation proportions, calculated by performing matrix corrections on maps of X-ray intensities, are used to study the microstructure of the symplectites.

Key words: dehydration; garnet granulite; hornblende–clinozoisite and clinopyroxene–kyanite symplectites; lower crust; New Zealand.

INTRODUCTION

Symplectite textures are commonly interpreted in terms of simultaneous growth of two or more minerals. Symplectite textures may form via a number of mechanisms. Among them are reaction during: (1) cooling following the metamorphic peak; (2) isothermal decompression of a terrane or (3) a transient temperature increase (e.g. Clarke & Powell, 1991). Symplectite textures have been used to infer *P–T* paths by determining the positions of the reactions involved in *P–T* space (e.g. Ellis *et al*., 1980; Droop & Bucher-Nurminen, 1984; Sandiford *et al*., 1987). More recently, studies have included an examination of hydration replacement textures that formed during cooling or decompression (e.g. Carson *et al*., 1999, 2000). We present evidence for the hydration of coarse-grained garnet–clinopyroxene granofels to form symplectic intergrowths of hornblende–clinozoisite and the subsequent dehydration of coarse-grained hornblende–clinozoisite assemblages to form garnet, clinopyroxene and symplectic intergrowths of (1) clinopyroxene and kyanite, and (2) clinozoisite, quartz, kyanite and plagioclase. The replacement textures are described for mafic granofels of the Arthur River Complex, which formed within the contact aureole of the Early Cretaceous Western Fiordland Orthogneiss batholith at Mt Daniel, Fiordland, New Zealand. We present a technique for analysing fine-grained symplectites using maps of oxide weight percent and cation proportions, calculated by performing matrix corrections on maps of X-ray intensities (after Clarke *et al*., 2001). Microstructural relationships and microprobe analyses are used to infer equations for the metamorphic reactions. However, this gives no information on the mechanism(s) controlling the reaction sequence and thus we present a T–M_{H_2O} pseudosection for the model system CNFMASH (CaO–Na_2O–FeO–MgO–Al_2O_3–SiO_2–H_2O) to infer that the textures were controlled by hydration and dehydration of the mafic granofels and gneisses.

REGIONAL GEOLOGY

The geology of the south island of New Zealand can be divided into three domains. Eastern and Western Provinces (Landis & Coombs, 1967; Bishop *et al*.,

* Now at: Dept. of Geological Sciences and Institute for Geophysics, Jackson School of Geosciences, University of Texas at Austin, Texas, USA.

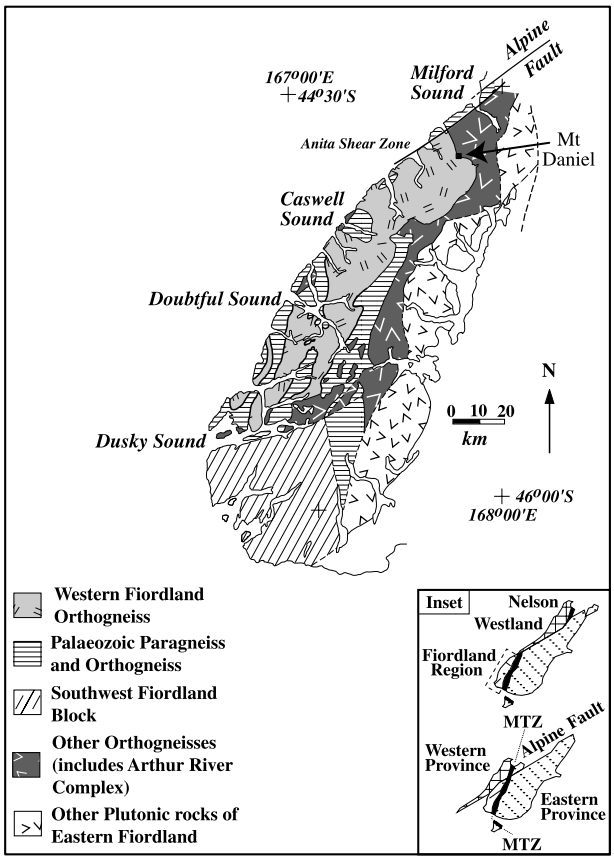

Fig. 1. Geological map of Fiordland showing major lithological divisions (after Bradshaw, 1990). Mt Daniel is located at the northern contact of the Western Fiordland Orthogneiss batholith. Inset shows the present-day (top) and pre-Cenozoic (bottom) configuration of the South Island, which places the Westland–Nelson region adjacent to Fiordland.

1985; inset Fig. 1) are separated by a belt of rocks referred to as the Median Tectonic Zone (Kimbrough *et al*., 1993, 1994; MTZ inset Fig. 1) or Median Batholith (Mortimer *et al*., 1999). Western Province rocks include Lower Palaeozoic paragneisses, cut by Devonian, Carboniferous and Cretaceous granitoids (Muir *et al*., 1996; Wandres *et al*., 1998). The Arthur River Complex (Bradshaw, 1990; Fig. 1) is a belt of granulite facies orthogneiss that lies at the boundary between the Median Tectonic Zone and Western Province rocks in northern Fiordland (Fig. 1). It is heterogeneous in rock-type and structure (Clarke *et al*., 2000), and Mesozoic and Palaeozoic ages have been inferred for orthogneiss units from this belt (Mattinson *et al*., 1986; Bradshaw, 1990). In Milford Sound, the Arthur River Complex includes dioritic and trondhjemitic gneisses of the Harrison Gneiss and gabbroic gneisses of the Pembroke Granulite and Milford Gneiss (Wood, 1972; Blattner, 1991; Clarke *et al*., 2000). The Anita Shear Zone forms the northwestern boundary of the Arthur River Complex; rocks of the Western Province lie northwest of the shear zone (Hill, 1995a,b; Klepeis *et al*., 1999; Fig. 1). Rocks of the Western Province and Median Tectonic Zone were intruded by the 126–116 Ma Western Fiordland Orthogneiss (Bradshaw, 1990; Kimbrough *et al*., 1994; Fig. 1). Intrusive relationships are preserved at Mt Daniel (Bradshaw, 1990; Fig. 1) with the Arthur River Complex retaining evidence of mid-crustal high-T metamorphism and partial melting within the contact aureole of the batholith as discussed below.

FIELD RELATIONS AND PETROGRAPHY

The Arthur River Complex at Milford Sound is a well-foliated gabbroic and dioritic orthogneiss that experienced up to five deformation events during the Early Cretaceous (Blattner, 1978, 1991; Klepeis *et al*., 1999; Clarke *et al*., 2000). At Mt Daniel, the Arthur River Complex lacks the pervasive north-striking, steeply dipping, foliation observed in Milford Sound (Blattner, 1991; Clarke *et al*., 2000), and mostly contains pods of garnet–clinopyroxene granofels enveloped by weakly to moderately well-foliated (S1) hornblende–clinozoisite gneiss.

Pods of garnet–clinopyroxene granofels up to 50 m across are formed from coarse-grained (up to 4 mm) garnet, clinopyroxene, quartz and titanite (Fig. 2a). Mineral modes obtained by point counting are presented in Table 1. Trondhjemite veins (Fig. 2b), up to a few centimetres wide, cut the pods and are continuous with leucosome that encloses idioblastic garnet (white arrow, Fig. 2b). The trondhjemite veins also cut the Western Fiordland Orthogneiss at the contact with the Arthur River Complex, where approximately 1 m-wide rafts of Arthur River Complex occur within the Western Fiordland Orthogneiss (Fig. 2c). We infer that the idioblastic garnet and veins formed by the incongruent melting of dioritic to gabbroic Arthur River Complex wall rocks during intrusion of the Western Fiordland Orthogneiss. The partial melting textures, limited plagioclase in the mafic granofels, the trondhjemite veins and limited retrogression are consistent with there having been considerable melt escape (see also Daczko *et al*., 2001).

The hornfelsic pods are enveloped by hornblende–clinozoisite assemblages that occur either in symplectites or as moderately well-foliated recrystallized assemblages (S1). S1 is east-striking, dips moderately to the south and is defined by coarse-grained (up to 2 mm long) hornblende and clinozoisite. S1 contains a weakly developed hornblende lineation that plunges moderately to the west. The hornblende–clinozoisite mafic gneiss consists of approximately 6% quartz, plagioclase, titanite and rutile, in addition to 61% hornblende and 33% clinozoisite (Table 1).

Symplectic intergrowths of hornblende and clinozoisite are found at the margins of the hornfelsic pods in hydration zones that may be up to 50 mm wide (Fig. 2d). Hornblende and clinozoisite form elongate blades (up to 1 mm long) in symplectites that radiate

out from grains of garnet and clinopyroxene (Fig. 2d). Texturally, clinopyroxene was replaced before garnet. Titanite appears unaffected, and is enveloped by the symplectites in most samples (Fig. 2d). However, in sample Dan16, titanite is partially pseudomorphed by rutile (Fig. 2e). Two reaction sequences are possible: (1) titanite in sample Dan16 was partially pseudomorphed by rutile concurrent with the development of the symplectites; or (2) rutile pseudomorphs after titanite postdate the hornblende–clinozoisite symplectites and formed during loading to deeper crustal levels (Bradshaw, 1989; Clarke *et al.*, 2000). From the observation that titanite appears most commonly unaffected by the hornblende–clinozoisite symplectites (Fig. 2d), we prefer the second scenario. The mode of quartz decreases with the extent of symplectite development, consistent with quartz being a reactant in the metamorphic reaction (Table 1). On the basis of these textures it is inferred that the following reaction controlled symplectite development:

$$\text{garnet} + \text{clinopyroxene} + \text{quartz} + H_2O = \text{hornblende} + \text{clinozoisite} \quad (1)$$

S1 is cut by rare, generally steeply dipping fractures that may or may not be filled with trondhjemite veins. These veins are not linked to leucosome in the garnet–clinopyroxene granofels and define a second veining event. Zones of bleached rock, generally < 65 mm wide, lie parallel and adjacent to the fractures and veins (Fig. 2f). Within the bleached areas (hereafter referred to as garnet reaction zones), S1 hornblende and clinozoisite are replaced by garnet–clinopyroxene–rutile assemblages (Fig. 2g). Garnet and clinopyroxene are commonly observed to mantle clinozoisite and hornblende grains, respectively. This is similar to a

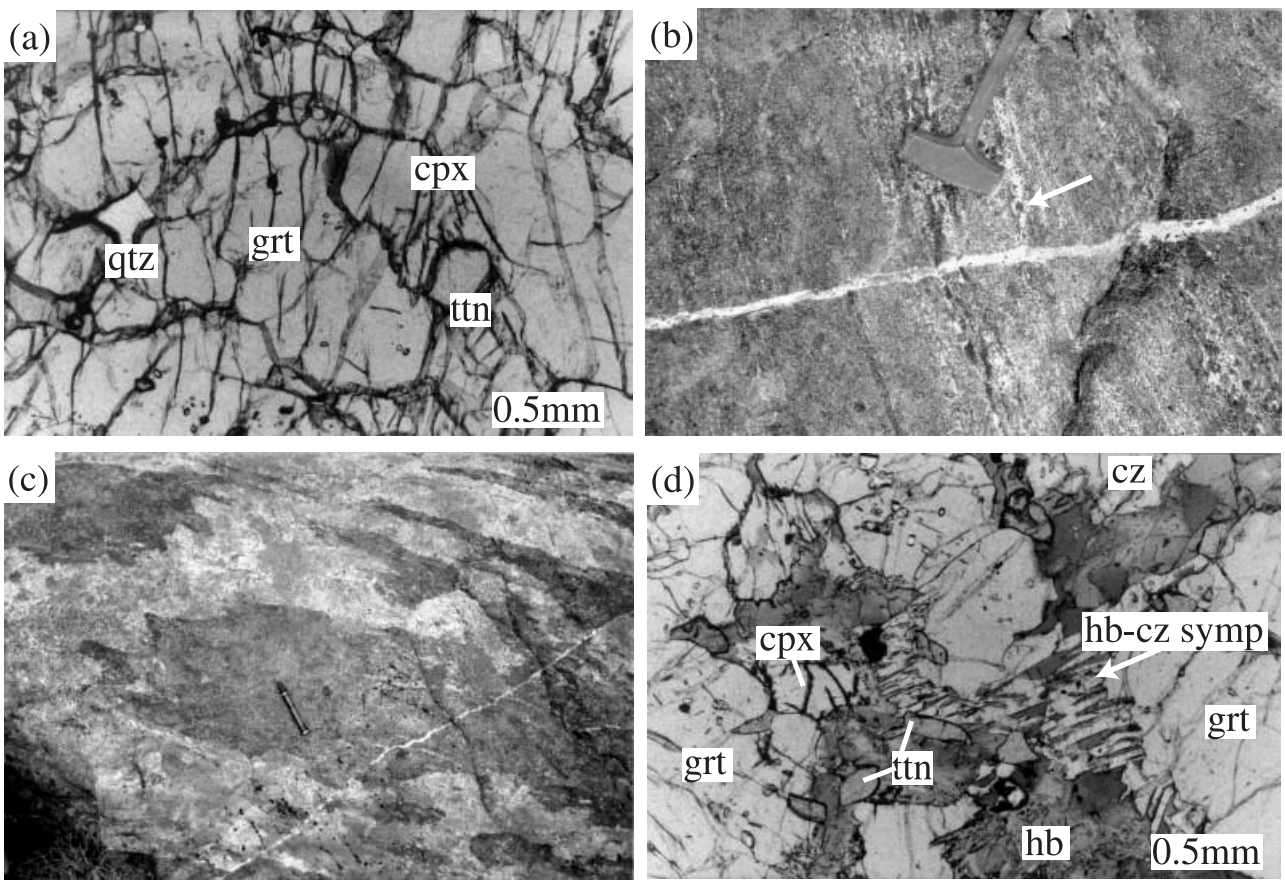

Fig. 2. (a) Photomicrograph of coarse-grained garnet–clinopyroxene granofels from sample Dan17. (b) Trondhjemite vein cuts garnet–clinopyroxene hornfels. The vein is linked to garnet surrounded by leucosome (white arrow). (c) Trondjemite vein cuts the Western Fiordland Orthogneiss and enclosed rafts of Arthur River Complex country rock. (d) Photomicrograph of hornblende–clinozoisite symplectites that partially pseudomorph garnet and clinopyroxene in sample Dan17. Note the stable lenticular titanite grains within the replacement textures. (e) Photomicrograph of rutile pseudomorphs after titanite in hornblende–clinozoisite symplectites from sample Dan16. (f) Fractures and veins that cut the hornblende–clinozoisite mafic gneiss. Garnet reaction zones (bleached looking area) are developed parallel and adjacent to the veins and fractures. (g) Photomicrograph of garnet reaction zone sample Dan18. Garnet–clinopyroxene-rutile assemblages and fine-grained symplectic intergrowths partially to completely pseudomorph hornblende and clinozoisite. (h) Photomicrograph of symplectic intergrowths of clinopyroxene-kyanite (symp1) and clinozoisite-quartz-kyanite-plagioclase (symp2) after hornblende and clinozoisite, respectively, in sample Dan18.

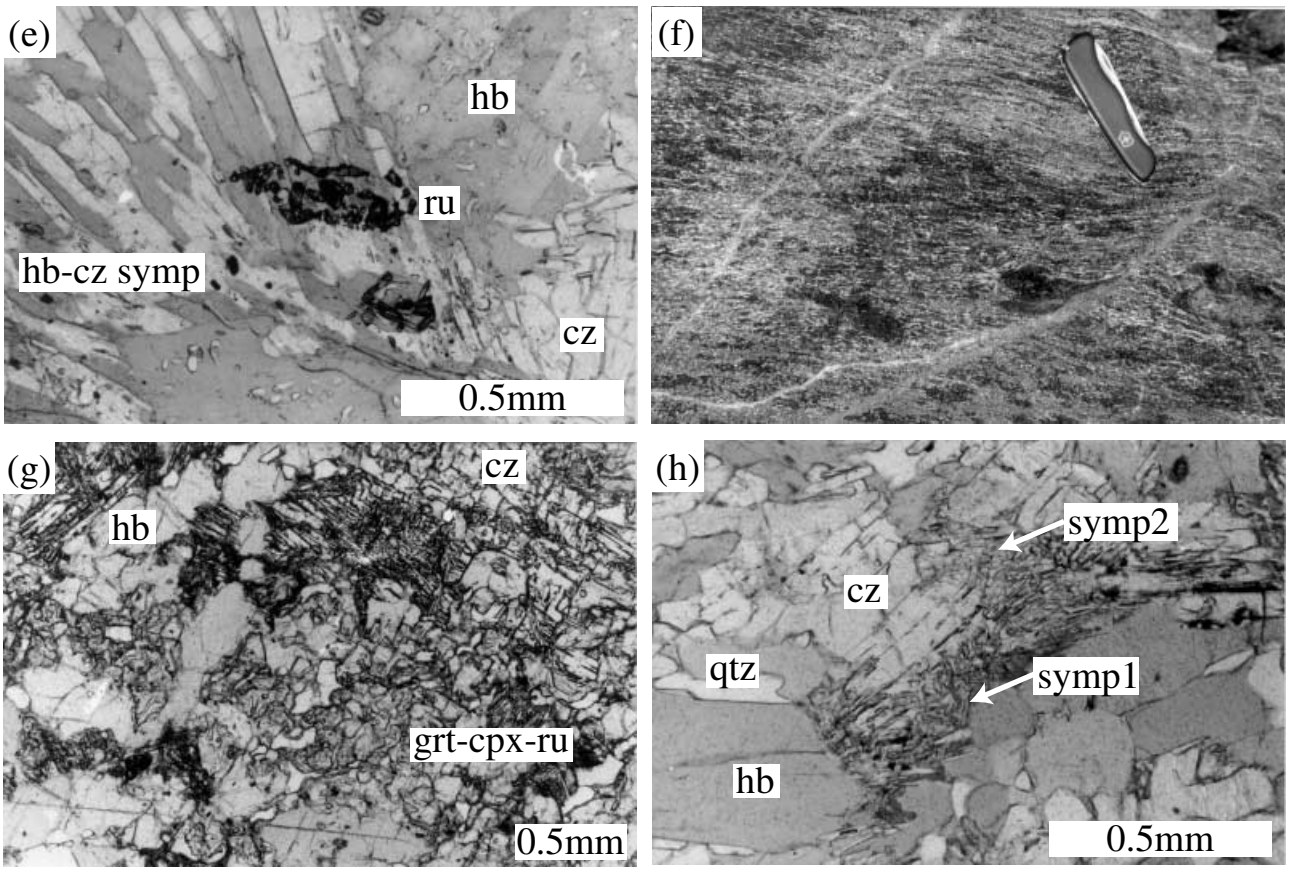

Fig. 2. (*Cont'd*).

Table 1. Modes of the garnet–clinopyroxene (grt–cpx) hornfels (Dan16), hydrated hornblende–clinozoisite equivalents (Dan17), and garnet reaction zone (Dan18), obtained by point counting, using an optical microscope. 500 points counted in each section.

	Dan16		Dan17		Dan18	
Sample	grt-cpx (partly hydrated)	Hydrated Zone	grt-cpx granofels	Hydrated Zone	hb-cz gneiss	Garnet Reaction Zone
Grt	50.2	0	52.6	0	0	27.2
Cpx	27	0	41.2	0	0	18.2
Hb	12.4	61.4	0	61.4	58.8	23
Cz	5.2	33.4	0	31.4	11.8	6.6
Qtz	2	0.8	2.2	0.4	5.6	6.6
Ttn	3	0.4	3.4	1.6	0	0
Rt	0	1.4	0	1.8	2	2
Plag	0.2	2.6	0.6	3.4	0	0
Cz-q-ky-plag symplecite	0	0	0	0	9	3.8
Cpx-ky symplecite	0	0	0	0	12.8	12.6

reversal of reaction (1) but most probably occurred at higher pressure, given the presence of rutile and other observations presented below. On the margins of the garnet reaction zones, S1 hornblende is partially replaced by fine-grained symplectic intergrowths of clinopyroxene and kyanite (symp1, Fig. 2h) and S1 clinozoisite is partially replaced by fine-grained symplectic intergrowths of clinozoisite, quartz, kyanite and plagioclase (symp2, Fig. 2h). Single grains in the symplectite textures are approximately 10 μm wide and 60 μm long. The minerals in the symplectites are too fine-grained and/or intricately intergrown for investigation using the optical microscope and were identified using back-scattered electron images and electron microprobe analyses. The kyanite-bearing symplectic intergrowths are most commonly observed at grain boundaries between S1 hornblende and clinozoisite. In parts of the sample where the replacement textures are extensively developed, S1 clinozoisite has been totally replaced by clinozoisite–quartz–kyanite–plagioclase symplectites. The persistence of clinozoisite in the symplectic intergrowths is inferred to reflect a modal shift in clinozoisite. On the basis of these textures we suggest that the following reaction controlled their formation:

$$\text{hornblende} + \text{clinozoisite} = \text{clinopyroxene} + \text{kyanite} + H_2O \quad (2)$$

$$\text{hornblende} + \text{clinozoisite} = \text{clinopyroxene} + \text{kyanite} + \text{quartz} + \text{plagioclase} + H_2O \quad (3).$$

QUANTITATIVE CATION MAPPING

In this section the microstructure of the fine-grained symplectite textures is examined using maps of oxide weight percent and cation proportions. The determination of the number of cations of Si, Al, Fe, Mn, Mg, Ca, Na and K for 24 oxygen was completed by first collecting raw intensity X-ray maps using a Cameca SX50 microprobe at the University of New South Wales with an accelerating voltage of 15 kV and a beam width of 1–3 μm. Eight X-ray intensity maps were collected in two sessions using four wavelength dispersive spectrometers. The element maps were collected with a 300-ms count time at each point and a 4-μm step size between points. The raw intensity maps were converted to maps of oxide weight percent by using the α-factor approach of Bence & Albee (1968) for matrix correction (Clarke *et al*., 2001). The matrix correction produces oxide weight percent data that were then recalculated to give cation proportions (on 24 oxygen). The oxide weight percent data were analysed to identify specific minerals and appropriate threshold values of cation proportions were used to calculate mineral modes. Two areas were analysed for the assemblages in the garnet reaction zones, including the fine-grained symplectites in sample Dan18.

Figure 3 shows maps of oxide weight percent for a well-developed portion of a garnet reaction zone in sample Dan18. The figure shows clinopyroxene and garnet poikiloblasts (0.3×0.4 mm) with very fine-grained (10–50 μm across) clinopyroxene inclusions (arrow 1) that have replaced S1 hornblende and clinozoisite. Hornblende is mantled by clinopyroxene that shows a minor core to rim increase in jadeite content (arrow 2, Na_2O increases by approximately 1 weight percent). Quartz appears unaffected and is probably not involved in the development of the replacement textures.

Figure 4 shows maps of oxide weight percent for the edge of a garnet reaction zone in sample Dan18. Garnet and clinopyroxene, texturally similar to that in Fig. 3, are located at the top of Fig. 4. Clinopyroxene mantles on S1 hornblende (arrow 1) show a core to rim increase in jadeite content (arrow 5; Na_2O increases from approximately 2 weight percent in the core to approximately 3 weight percent in the rim). Garnet mantles on S1 clinozoisite (arrow 4) show no evidence of compositional zoning. A clinozoisite grain aligned within S1 (0.5×1 mm grain labelled cz on the Al_2O_3 map, Fig. 4) contains quartz that appears to lie along mineral cleavage planes (see SiO_2 map, Fig. 4). This grain is in contact with hornblende to the right in the figure (arrow 2) where it has reacted with S1 hornblende to produce fine-grained clinozoisite, quartz and minor plagioclase. Clinozoisite in a second textural setting is fine-grained and symplectically intergrown with quartz, kyanite and plagioclase (arrow 3, Fig. 4). Kyanite is generally restricted to the cores of the clinozoisite-bearing symplectic intergrowths.

Figure 5 shows maps of oxide weight percent for sample Dan18, collected a few centimetres outside the garnet reaction zone mapped in Fig. 4. The figure shows hornblende partially pseudomorphed by symplectic intergrowths of clinopyroxene and kyanite (arrow 2). Adjacent to the clinopyroxene and kyanite symplectites is a structured clinozoisite-bearing symplectite with kyanite generally restricted to the core (arrows 1 & 3), similar to that described in Fig. 4. Arrow 1 points to an area of the map containing symplectic intergrowths of clinozoisite and quartz. Arrow 3 points to an area of the map with symplectic intergrowths of clinozoisite, quartz, kyanite and plagioclase.

Figure 6 shows a simplified line drawing of the textures compiled from the maps of oxide weight percent shown in Fig. 5. Plagioclase is very fine-grained and was excluded for simplicity, but may be seen in Fig. 4. Sub-areas of the oxide weight percent maps (Area 1 in Fig. 4; Areas 2 and 3 in Fig. 6) and an area containing well-developed garnet–clinopyroxene replacement textures were selected for modal analysis. The areas selected for modal analysis are very small (each subarea covers about 0.04 mm^2) and hence the results should only be used as a guide. Each subarea of the oxide weight percent maps was isolated and recalculated to give cation proportions (on 24 oxygen). Appropriate compositional threshold values were chosen to isolate specific minerals in each subarea. The threshold values were chosen to ensure that each pixel was identified as a certain mineral and counted only once. The total counts for each mineral were divided by the total number of pixels in the subarea to give an estimate of mode. Table 2 presents the modes determined for this analysis. The analysis showed that the clinopyroxene and kyanite symplectites consist of approximately 75% clinopyroxene and 25% kyanite. The analysis also showed that modal content of the clinozoisite-bearing symplectites varied considerably. Area 1 contained over 70% clinozoisite, whereas Area 3 contained $<30\%$ clinozoisite. Similarly, the modes of quartz, kyanite and plagioclase increased dramatically between Area 1 and Area 3. Though this type of comparative analysis indicates that S1 clinozoisite broke down to form symplectic clinozoisite with quartz, kyanite and plagioclase, the range in mineral proportions is consistent with the modes within the symplectites having evolved during their formation.

The final analysis using the element maps involves estimating and comparing bulk compositions for selected areas. We selected an area of the oxide weight percent map shown in Fig. 5 that consisted of only hornblende and calculated the average composition of the area by taking the mean of the data. Each elemental oxide is within 1.5 weight percent and 0.25 cations of the data obtained by the electron microprobe (compare average hornblende data in Table 3 with the hornblende analysis in the fifth

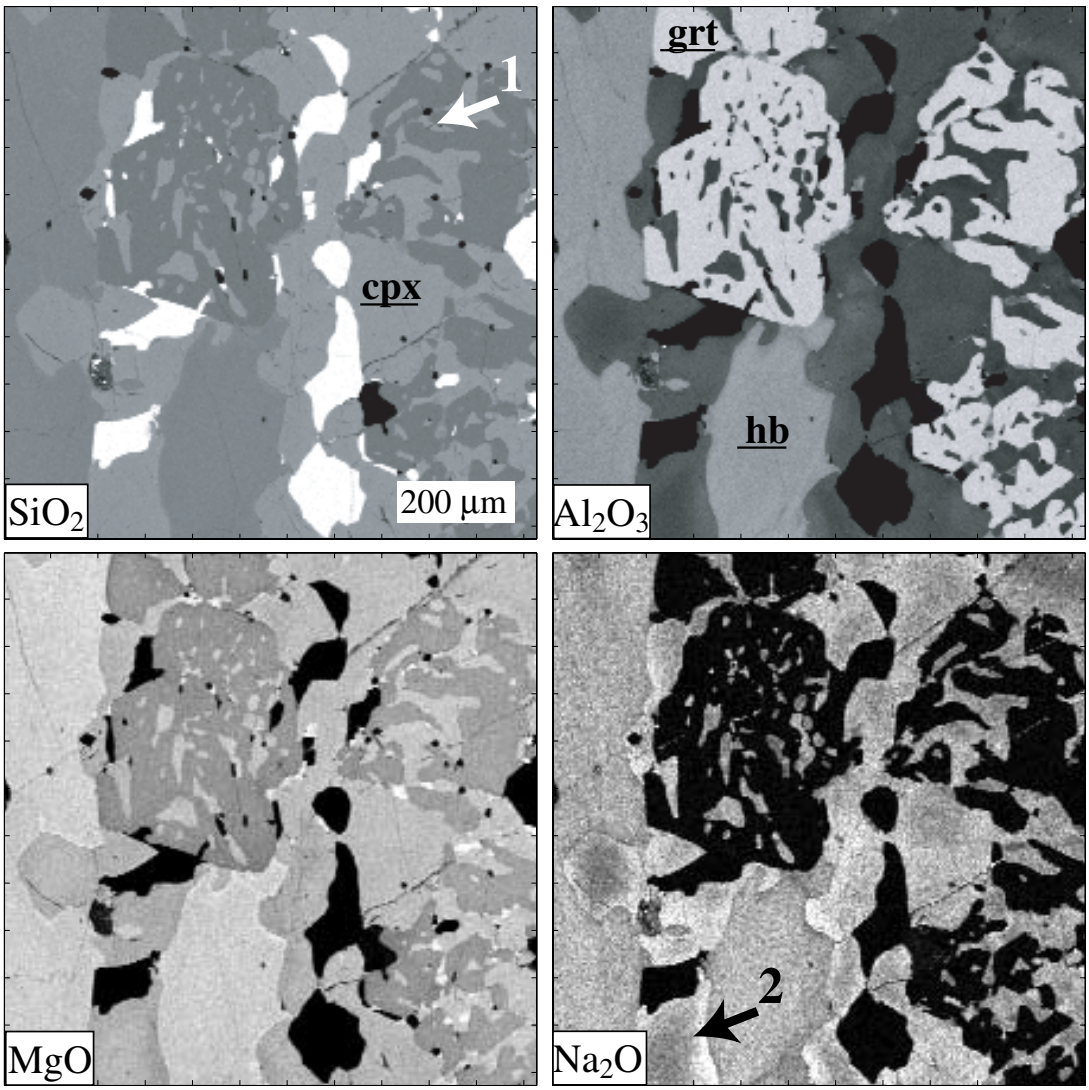

Fig. 3. Matrix corrected oxide weight percent maps for SiO_2, Al_2O_3, MgO and Na_2O in garnet reaction zone sample Dan18. The maps are approximately 900 × 900 μm. Grey scale is black for minimum elemental concentration and white for maximum elemental concentration. Minimum and maximum ranges: SiO_2 is 0–100 wt.%, Al_2O_3 is 0–30 wt.%, MgO is 0–20 wt.%, Na_2O is 0–4 wt.%. The white coloured mineral on the SiO_2 map is quartz. The medium-grey mineral on the SiO_2 map labelled 'cpx' is clinopyroxene. The brightest mineral on the Al_2O_3 map labelled 'grt' is garnet. The medium-grey mineral on the Al_2O_3 map labelled with 'hb' is hornblende. Arrow labelled with '1' points to clinopyroxene inclusions in a garnet poikiloblast. Arrow labelled with '2' points to a clinopyroxene grain that shows core to rim increase in jadeite content (increase of approximately 1 weight percent Na_2O).

column of Table 4). The average composition of the clinopyroxene and kyanite data in Area 2 was calculated, also by taking the mean. A comparison of the average compositions of each of these areas suggests that the symplectites are slightly enriched in Si, Al and Ca and slightly depleted in Fe and Mg (Table 3). This indicates that there was a component of element mobility during development of the clinopyroxene–kyanite symplectites. This is discussed further below.

A similar analysis for the clinozoisite-bearing symplectites yielded an average clinozoisite composition within 1.5 weight percent and 0.95 cations of the data obtained by the electron microprobe. The comparison between the average composition of the symplectites and the average composition of the clinozoisite suggests that the symplectites are enriched in Si and depleted in Ca. This analysis suggests that the replacement of S1 hornblende by symplectic intergrowths of clinopyroxene and kyanite and S1 clinozoisite by symplectic intergrowths of clinozoisite, quartz, kyanite and plagioclase were not isochemical. Silica, and possibly Ca, were mobile during symplectite development, suggesting that the rest of the rock was at least partly involved in their formation. Though less well constrained, Fe and to a lesser extent Mg were also mobile during development of the replacement textures.

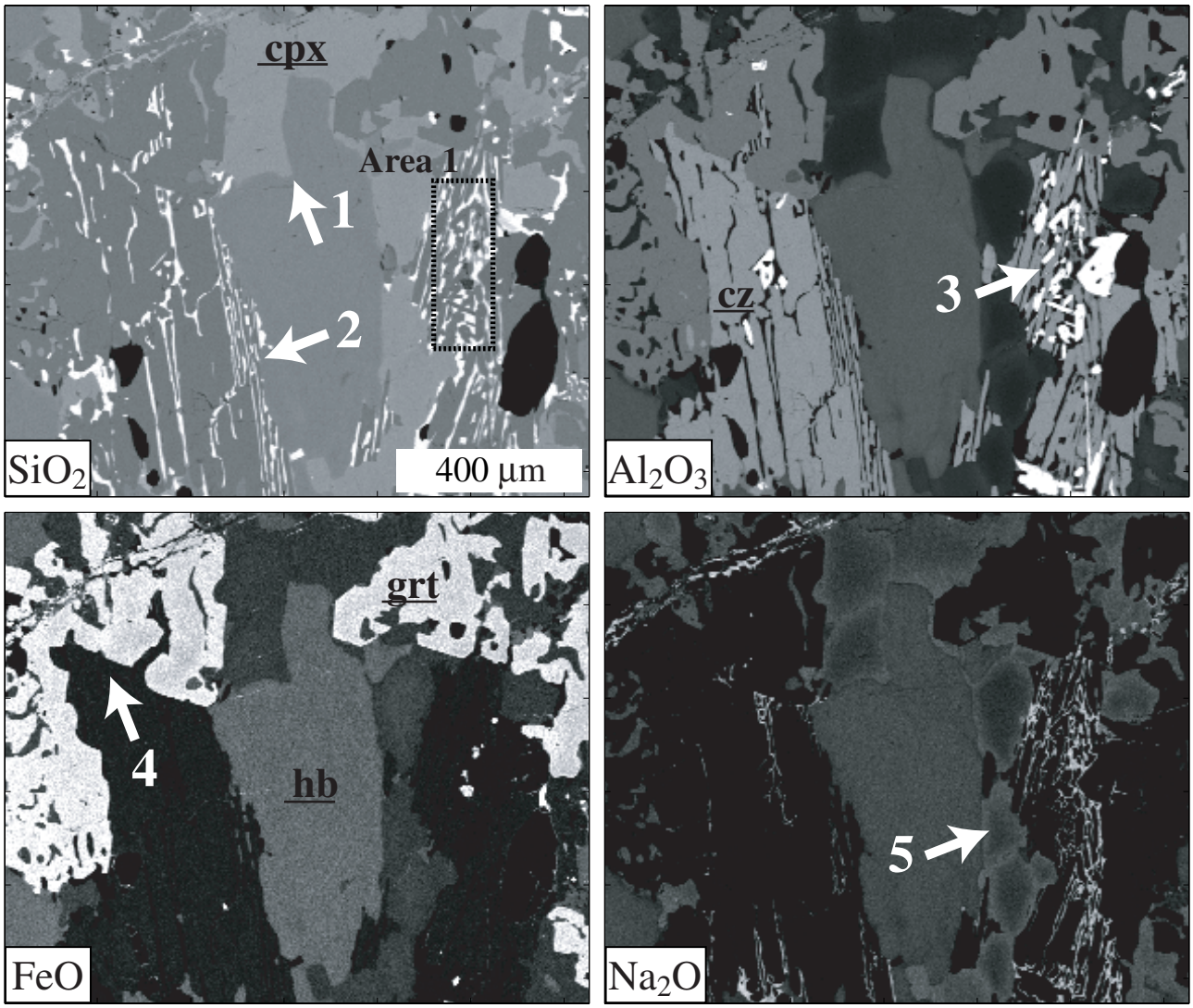

Fig. 4. Matrix corrected oxide weight percent maps for SiO_2, Al_2O_3, FeO and Na_2O at the edge of a garnet reaction zone in sample Dan18. The maps are approximately 1100 × 1300 μm. Grey scale is black for minimum elemental concentration and white for maximum elemental concentration. Minimum and maximum ranges: SiO_2 is 0–100 wt.%, Al_2O_3 is 0–63 wt.%, FeO is 0–20 wt.%, Na_2O is 0–13 wt.%. The white coloured mineral on the SiO_2 map is quartz. The medium-grey mineral on the SiO_2 map labelled 'cpx' is clinopyroxene. The white mineral on the Al_2O_3 map is kyanite. The medium-grey mineral on the Al_2O_3 map labelled with 'cz' is clinozoisite. The brightest mineral on the FeO map labelled 'grt' is garnet. The dark grey mineral on the FeO map labelled 'hb' is hornblende. The brightest mineral on the Na_2O map is plagioclase. Arrow labelled with '1' points to clinopyroxene mantle on hornblende. Arrow labelled with '2' points to a symplectic intergrowth of clinozoisite, quartz and limited plagioclase. Arrow labelled with '3' points to a symplectic intergrowth of clinozoisite, quartz, kyanite and plagioclase. Arrow labelled with '4' points to garnet mantle on clinozoisite. Arrow labelled with '5' points to a clinopyroxene grain that shows core to rim increase in jadeite. Modes for subarea labelled ''Area 1'' are presented in Table 4.

MINERAL CHEMISTRY AND THERMO-BAROMETRY

In this section we outline the mineral chemistry of the textures described above. These data are used to estimate metamorphic conditions that accompanied the development of the textures. Representative electron microprobe analyses of minerals from the garnet–clinopyroxene hornfels (sample Dan16) and garnet reaction zone (sample Dan18) are presented in Table 4.

Large garnet grains from the garnet–clinopyroxene hornfels are unzoned grossular- and pyrope-rich almandine with $Alm_{43}Spss_1Py_{25}Gr_{30}$ where Alm = 100 Fe/(Fe + Mg + Mn + Ca), Spss = 100 Mn/(Fe + Mg + Mn + Ca), Py = 100 Mg/ (Fe + Mg + Mn + Ca) and Gr = 100 Ca/ (Fe + Mg + Mn + Ca). Garnet in the garnet reaction zones has higher proportions of pyrope, lower proportions of almandine, and grossular values similar to garnet in the hornfels with $Alm_{34}Spss_1Py_{33}Gr_{31}$. Garnet in the garnet reaction zones may also be almandine-rich

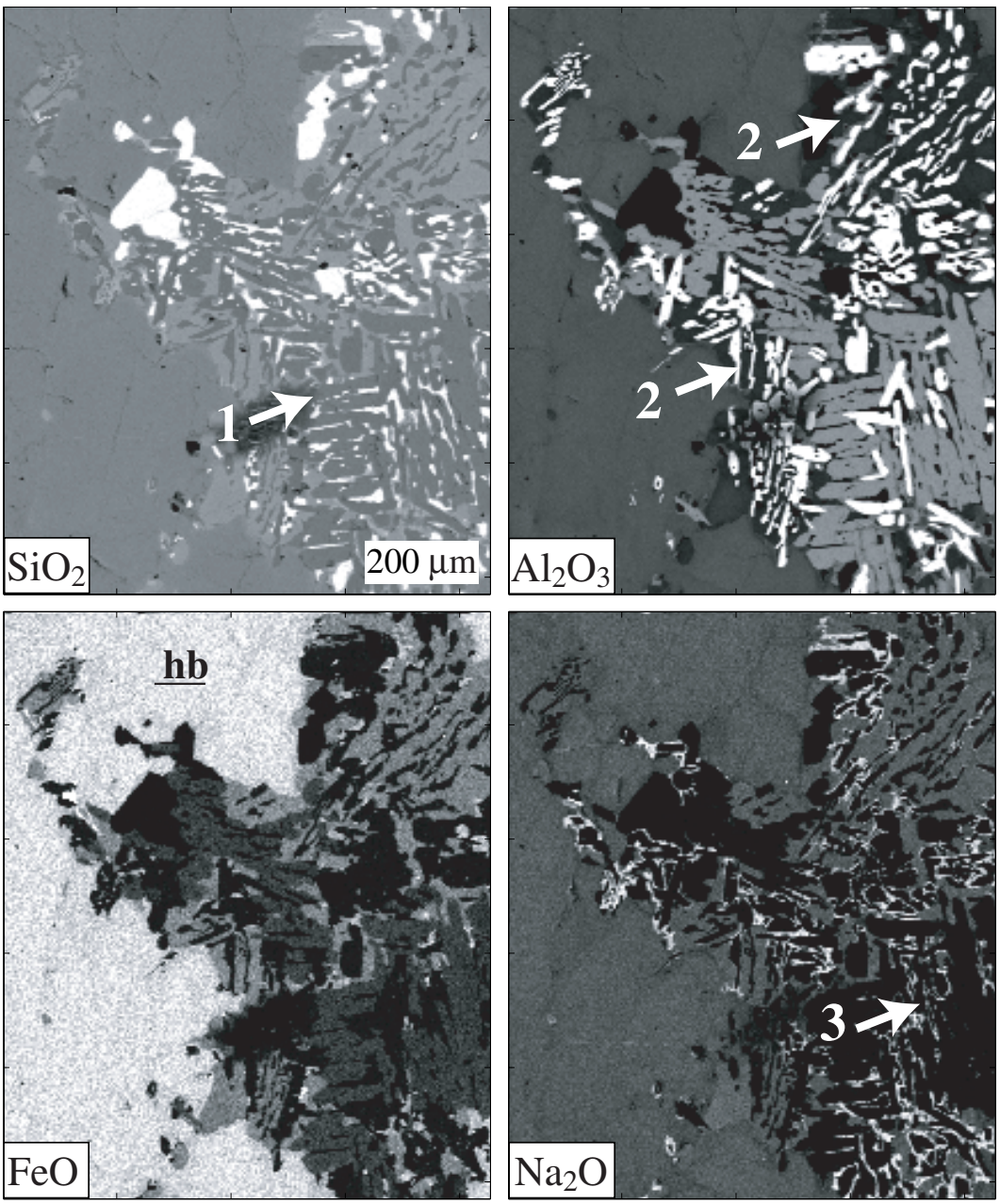

Fig. 5. Matrix corrected oxide weight percent maps for SiO_2, Al_2O_3, FeO and Na_2O outside of a garnet reaction zone in sample Dan18. The maps are approximately 1050 × 850 μm. Grey scale is black for minimum elemental concentration and white for maximum elemental concentration. Minimum and maximum ranges: SiO_2 is 0–100 wt.%, Al_2O_3 is 0–63 wt.%, FeO is 0–12 wt.%, Na_2O is 0–10 wt.%. The white coloured mineral on the SiO_2 map is quartz. The white mineral on the Al_2O_3 map is kyanite. The medium-grey mineral on the Al_2O_3 map is clinozoisite. The darkest mineral on the Al_2O_3 map is clinopyroxene. The brightest mineral on the FeO map labelled 'hb' is hornblende. The brightest mineral on the Na_2O map is plagioclase. Arrow labelled with '1' points to a symplectic intergrowth of clinozoisite, quartz and limited plagioclase. Arrows labelled with '2' point to symplectic intergrowths of clinopyroxene and kyanite. Arrow labelled with '3' points to a symplectic intergrowth of clinozoisite, quartz, kyanite and plagioclase.

and grossular-rich pyrope with $Alm_{33}Spss_1Py_{40}Gr_{27}$. Large clinopyroxene grains from the garnet–clinopyroxene hornfels are unzoned and have $X_{Fe} = [Fe/(Fe + Mg)] = 0.21$–$0.22$. When calculated using the method of Cawthorn & Collerson (1974), hornfelsic clinopyroxene has the general formula $Di_{65}Hed_{19}Ca\text{-}tsch_8Jd_9$. Clinopyroxene in the garnet reaction zones has lower X_{Fe} and higher jadeite content with $X_{Fe} = 0.11$–0.20, $Di_{66}Hed_9Ca\text{-}tsch_8Jd_{17}$.

Hornblende in the hornblende–clinozoisite symplectites is richer in Fe and Al and poorer in Ti when compared to coarse-grained S1 hornblende in the hornblende–clinozoisite mafic gneiss. Symplectic hornblende is ferro-pargasite to pargasite (after Leake

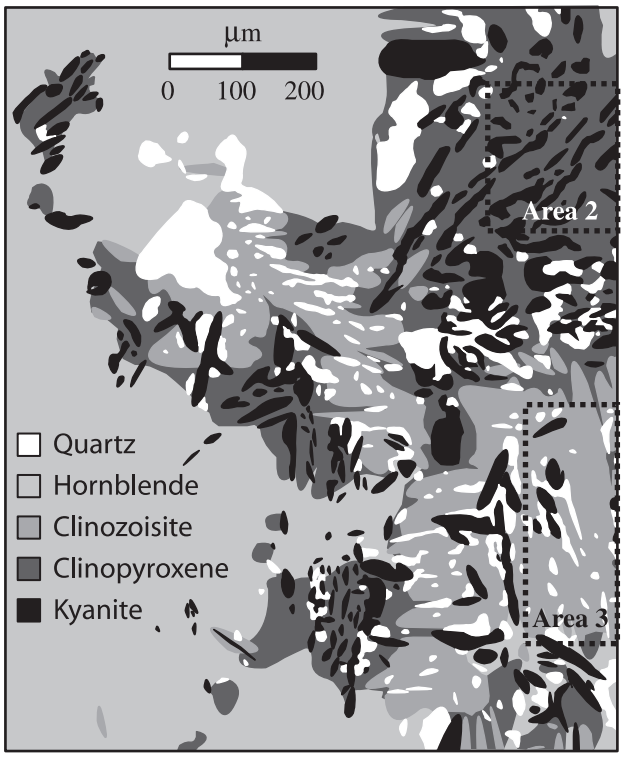

Fig. 6. Simplified mineral contoured line drawing of the oxide weight percent maps shown in Fig. 5. Plagioclase is very fine-grained and excluded for simplicity. Modes for subareas labelled 'Area 2' and 'Area-3' are presented in Table 4.

et al., 1997) with $X_{Fe} = 0.49–0.56$. Hornblende in the hornblende–clinozoisite mafic gneiss is pargasite with $X_{Fe} = 0.29–0.41$. Ferric iron in clinozoisite analyses was calculated assuming two-site ordering with a total of six Si, Al and Fe^{3+} cations per 12.5 oxygen. Clinozoisite in the hornblende–clinozoisite symplectites is pistacite-rich with cz = [Al-2] = 0.25–0.44. S1 clinozoisite grains in the hornblende–clinozoisite mafic gneiss are pistacite-poor with cz = 0.74–0.92. Kyanite generally contains less than 1 weight percent Fe_2O_3. The composition of plagioclase varies with textural setting. It is generally oligoclase with $X_{An} = [Ca/(Ca + Na)] = 0.15–0.24$.

Table 2. Modes for symplectites in sample Dan18, determined by image analysis of cation maps. Areas 1, 2 and 3 are labelled on Figs 4 and 6.

Sample	Dan 18 Grt-cpx (garnet reaction zone)	Cpx-Ky (Area 2)	Cz-Qtz-Ky-Plag (Area 1 less developed)	Cz-Qtz-Ky-Plag (Area 3 well developed)
Cpx	39.2	73.8	3.0	1.9
Grt	37.9	0	0	0
Hb	12.4	0	0	0
Cz	0	0	73.3	27.8
Qtz	10.5	1.1	9.0	20.6
Ky	0	25.1	8.4	27.8
Plag	0	0	6.3	21.9
Total points counted	82 500	2350	2720	2250
Area analysed (mm^2)	1.3200	0.0376	0.04352	0.0360

Table 3. Average compositions for selected areas of the maps of oxide weight percent. Cation proportions are calculated for the average data for 23 oxygen (hornblende and symplectic replacements) and 25 oxygen (clinozoisite and symplectic replacements) to allow comparison with data obtained from the electron microprobe (Table 4).

	Cpx-Ky symplecites		Cz-Qtz-Ky-Plag symplecites		
	Avg. Hb-	Avg. Area 2	Avg. Cz	Avg. Area 1	Avg. Area 3
SiO_2	43.7	49.7	40.0	46.2	53.2
Al_2O_3	16.2	21.4	32.3	29.2	31.6
FeO	9.9	3.8	1.6	2.0	1.2
MnO	0.3	0.3	0.0	0.2	0.1
MgO	13.4	9.1	0.1	0.9	0.4
CaO	10.1	13.4	22.5	17.1	8.3
Na_2O	2.2	2.3	0.0	0.7	1.6
K_2O	0.6	0.1	0.0	0.1	0.1
Total	96.4	100.1	96.5	96.4	96.5
Oxygen	23	23	25	25	25
Si	6.4	6.7	6.1	6.9	7.6
Al	2.8	3.4	5.9	5.2	5.3
Fe	1.2	0.4	0.2	0.2	0.1
Mn	0.0	0.0	0.0	0.0	0.0
Mg	2.9	1.8	0.0	0.2	0.1
Ca	1.6	1.9	3.7	2.8	1.3
Na	0.6	0.6	0.0	0.2	0.5
K	0.1	0.0	0.0	0.2	0.0
Total	15.6	14.8	15.9	15.7	14.9

Temperature estimates were made on the basis of the compositions of adjacent garnet and clinopyroxene grains for the garnet–clinopyroxene hornfels (sample Dan16) and garnet reaction zones (sample Dan18). The results of garnet–clinopyroxene thermometry are presented at the bottom of Table 4 (after Ellis & Green, 1979; Powell, 1985). For sample Dan16, within the contact aureole of the Western Fiordland Orthogneiss, we used an assumed pressure of 9 kbar for the thermometry on the basis of reported middle crustal emplacement levels for the batholith (e.g. Bradshaw, 1989; Clarke *et al.*, 2000). Changing the assumed pressure by ± 3 kbar resulted in a temperatures 30 °C above or below those presented below, suggesting that the choice of pressure is not critical. For sample Dan16, garnet–clinopyroxene thermometry yielded temperature estimates of >800 °C for P = 9 kbar. If a correction is made for Fe^{3+} in clinopyroxene, then the temperature estimates drop to 770–785 °C (Table 4). No plagioclase was found in samples of the garnet–clinopyroxene hornfels and hence it is not possible to provide a quantitative pressure estimate. For sample Dan18 (garnet reaction zone), garnet–clinopyroxene thermometry yielded temperature estimates of 775–790 °C for P = 12 kbar. The assumption of P = 12 kbar is made on the basis of conservative maximum pressures reported for garnet reaction zones in Fiordland (e.g. Clarke *et al.*, 2000). Changing the assumed pressure by ± 3 kbar produces temperature estimates 10–25 °C higher or lower than those presented for Dan18. The correction for Fe^{3+} in

Table 4. Representative electron microprobe analyses (weight percent oxide and cation data) for samples Dan16, Dan17 and Dan18. Data were collected on a Cameca SX50 microprobe at the University of New South Wales with an accelerating voltage of 15 kV and a beam width of 1–3 μm. Thermobarometric results for garnet–clinopyroxene thermometry (1. Ellis & Green, 1979; 2. Powell, 1985) and garnet–clinopyroxene-plagioclase-quartz barometry (3. Newton & Perkins, 1982) are presented at the bottom of the table.

	grt-cpx granofels		hb-cz symplectites		hb-cz mafic gneiss		Garnet reaction zones and symplectite textures					
	Grt	Cpx	Hb	Cz	Hb	Cz	Grt	Cpx	Ky	Plag	Hb	Cz
SiO_2	38.38	51.88	38.76	37.19	43.47	39.03	39.73	53.24	36.90	61.83	43.56	39.34
TiO_2	0.36	0.42	0.09	0.16	0.78	0.13	0.03	0.26	0.00	0.00	1.08	0.07
Al_2O_3	21.56	5.63	19.88	23.86	14.65	31.04	22.42	7.79	63.03	23.74	15.44	31.70
Cr_2O_3	0.11	0.03	0.09	0.01	0.05	0.00	0.05	0.03	0.00	0.01	0.03	0.01
FeO	20.64	6.26	16.46	11.08	10.36	2.68	16.68	3.20	0.52	0.19	10.07	2.45
MnO	0.71	0.08	0.28	0.20	0.14	0.03	0.51	0.03	0.00	0.00	0.15	0.07
MgO	6.78	12.21	7.38	0.08	12.89	0.08	9.11	12.73	0.02	0.00	12.83	0.08
CaO	11.39	21.13	11.09	22.63	11.31	23.95	11.84	20.57	0.02	4.91	10.83	23.82
Na_2O	0.05	1.94	2.14	0.02	1.95	0.02	0.03	2.73	0.00	8.64	2.62	0.01
K_2O	0.01	0.00	0.46	0.00	0.78	0.01	0.00	0.01	0.00	0.24	0.51	0.01
Total	99.99	99.58	96.63	95.23	96.38	96.97	100.40	100.59	100.49	99.56	97.12	97.55
oxygen	12	6	23	25	23	25	12.00	6.00	5.00	8.00	23.00	25.00
Si	2.96	1.92	5.86	6.17	6.39	6.05	2.98	1.91	0.99	2.75	6.33	6.05
Ti	0.00	0.01	0.01	0.02	0.09	0.02	0.00	0.01	0.00	0.00	0.12	0.01
Al	1.96	0.25	3.54	4.67	2.54	5.67	1.98	0.33	2.00	1.25	2.64	5.74
Cr	0.01	0.00	0.01	0.00	0.01	0.00	0.00	0.00	0.00	0.00	0.00	0.00
Fe	1.33	0.19	2.08	1.54	1.27	0.35	1.05	0.10	0.01	0.01	1.22	0.32
Mn	0.05	0.00	0.04	0.03	0.02	0.00	0.03	0.00	0.00	0.00	0.02	0.01
Mg	0.78	0.67	1.66	0.02	2.82	0.02	1.02	0.68	0.00	0.00	2.78	0.02
Ca	0.94	0.84	1.80	4.02	1.78	3.98	0.95	0.79	0.00	0.23	1.69	3.92
Na	0.01	0.14	0.63	0.01	0.56	0.01	0.00	0.19	0.00	0.75	0.74	0.00
K	0.00	0.00	0.09	0.00	0.15	0.00	0.00	0.00	0.00	0.01	0.10	0.00
Total	8.04	4.02	15.72	16.48	15.63	16.10	8.01	4.01	3.00	5.00	15.64	16.07
	No corr.	Fe^{3+} corr.					No corr.	Fe^{3+} corr.				
	835 °C_1	785 °C_1					791 °C_1	714 °C_1				
	821 °C_2	769 °C_2					775 °C_2	696 °C_2				
									13.9 kbar$_3$			

clinopyroxene reduced these temperature estimates to 700–715 °C (Table 4). Using the minimum thermometry result of 700 °C, the compositions of coexisting garnet, clinopyroxene, plagioclase and quartz in sample Dan18 indicates that $P = 13.9$ kbar from the method of Newton & Perkins (1982). The assemblage garnet, kyanite, plagioclase and quartz, also in sample Dan18, indicates that $P = 13.2$ kbar for $T = 700$ °C (after Newton & Haselton, 1981). Changing the assumed temperature by ± 100 °C results in pressure estimates approximately 1 kbar higher or lower than the results presented for Dan18.

T–M_{H_2O} pseudosection

The thermobarometric results indicate that the garnet reaction zones developed in the deep crust ($P = 13$ kbar) at elevated temperatures ($T >$ 700 °C). The available thermobarometric methods provide no way of estimating the temperature or pressure at which the hornblende–clinozoisite symplectites developed. However, the garnet–clinopyroxene hornfels developed at $T = 750$–800 °C, and this suggests that the hornblende–clinozoisite symplectites developed as the thermal aureole cooled between 800 and 700 °C. The petrological analysis of the reaction textures and the reactions presented above suggest that water played a vital role in the development of the hornblende–clinozoisite symplectites. In addition, the thermobarometric techniques that we used give no information with respect to the proportion of fluid that accompanied the development of the symplectites. Similarly, there is little information with respect to any changes in the proportion of fluid that accompanied the development of the symplectic intergrowths of clinopyroxene and kyanite and clinozoisite–quartz–kyanite–plagioclase.

An equilibrium approach is taken to the development of these textures and quantitative T–M_{H_2O} pseudosection that has been constructed in the model system CNFMASH (CaO–Na_2O–FeO–MgO–Al_2O_3–SiO_2–H_2O), using THERMOCALC (version 2.75) and the '20 April 1996' internally consistent thermodynamic data set (Powell *et al.*, 1998). Details of the use of THERMOCALC for grid and pseudosection construction are outlined in Powell *et al.* (1998). Minerals included in the construction of the grid are garnet (Grt), hornblende (Hb), paragonite (Pa), clinozoisite (Cz), kyanite (Ky), orthopyroxene (Opx), clinopyroxene (Cpx), plagioclase (Plag) and quartz (Qtz). Most of the activity models used in the calculations assume ideal mixing on all sites and are identical to those used by Powell *et al.* (1998). Where present, the fluid phase is assumed to be pure H_2O, as water was

the only volatile observed to be part of the paragenesis. However, it is possible that the dehydration textures were caused by the introduction of a CO_2-rich fluid along the fractures and veins. If this was the case, the primary effect appears to have been the removal of H_2O, rather than the addition of CO_2 to the bulk rock composition in the garnet reaction zones. In the T–M_{H_2O} diagram, M_{H_2O} is defined as the molar proportion of the component, H_2O, in the bulk composition (Guiraud *et al.*, 1996; Carson *et al.*, 1999; Clarke *et al.*, 2000). Figure 7(a) represents a T–M_{H_2O} pseudosection appropriate to the bulk composition of the garnet–clinopyroxene hornfels and hornblende–clinozoisite mafic gneiss. On the basis of a conservative peak estimate of pressure outlined above, it is drawn at fixed $P = 12$ kbar. Altering the fixed pressure to 13 kbar will move the horizontal boundaries of the divariant field containing the assemblage Pa, Grt, Hb, Plag, Cpx and H_2O up on the diagram by < 15 °C. Altering the fixed pressure will not move the other boundaries on the diagram up or down by more than a few degrees. Figure 7(a) is restricted to $T = 550$–700 °C, as nothing new appears on the diagram between 700 and 800 °C, and the water saturation line continues parallel to its trend, shown at the top of the diagram, up to 800 °C. The isobaric nature of the diagram is necessary in order to model the two variables considered most important (T & M_{H_2O}). The lack of zonation in garnet and minor zonation in clinopyroxene (Fig. 4) are consistent with a quasi-isobaric history during at least the development of the garnet reaction zones and symplectite textures. Minor variation in pressure during the evolution of the textures does not greatly affect the position of the fields on the diagram.

The rock composition used was obtained from XRF whole rock analyses, and varies (Fig. 7a) from CaO = 31.23, $Na_2O = 2.31$, FeO = 24.40, MgO = 22.52, $Al_2O_3 = 19.53$, $H_2O = 0.00$ ($M_{H_2O} = 0$) to CaO = 27.33, $Na_2O = 2.02$, FeO = 21.35, MgO = 19.71, $Al_2O_3 = 17.09$, $H_2O = 12.5$ ($M_{H_2O} = 0.125$). The pseudosection is drawn for quartz in excess, and illustrates the mineral evolution with respect to changing temperature and M_{H_2O}. A horizontal line on the diagram represents the addition or subtraction of H_2O at a given temperature. The indicated H_2O-saturation line is the limiting boundary beyond which any further increase of M_{H_2O} only increases the mode of

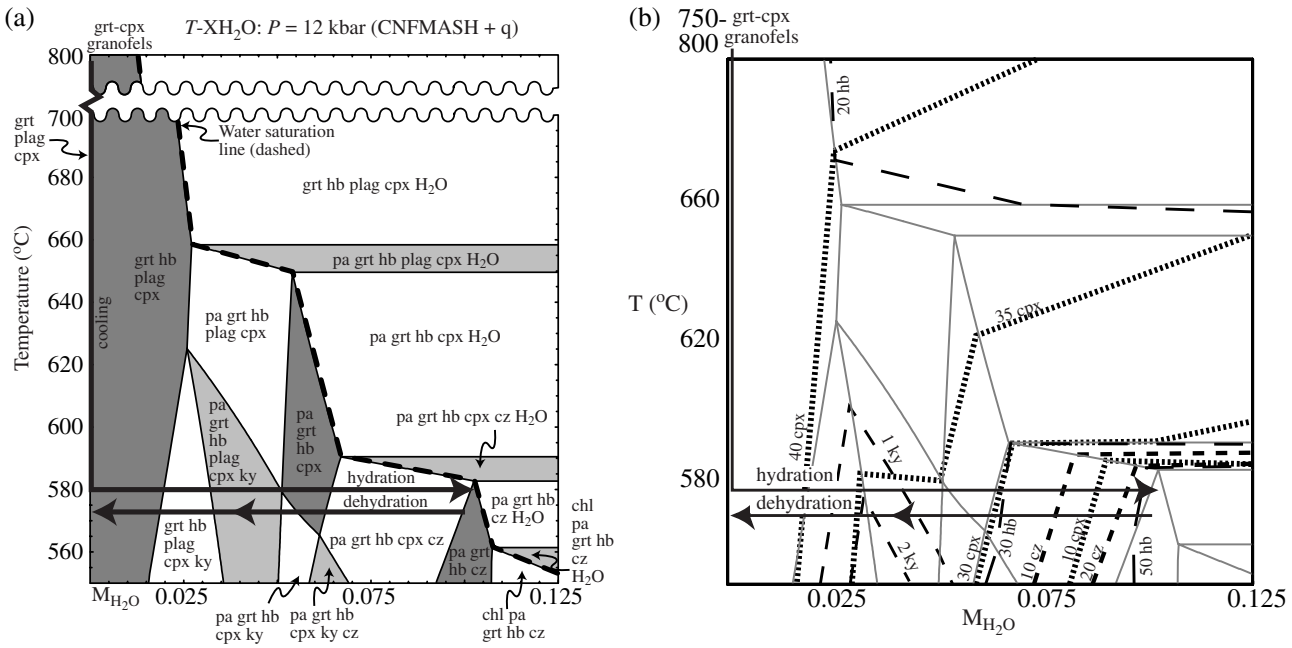

Fig. 7. (a) T–M_{H_2O} pseudosection for $P = 12$ kbar and $T = 550$–700 °C, constructed in the model system CNFMASH (CaO-Na_2O-FeO-MgO-Al_2O_3-SiO_2-H_2O), using THERMOCALC (version 2.75) and the '20 April 1996' internally consistent thermodynamic data set of Powell *et al.* (1998). The bulk rock composition was determined from XRF analysis and ranges in the model from CaO = 31.23, $Na_2O = 2.31$, FeO = 24.40, MgO = 22.52, $Al_2O_3 = 19.53$, $H_2O = 0.00$ ($M_{H_2O} = 0$) to CaO = 27.33, $Na_2O = 2.02$, FeO = 21.35, MgO = 19.71, $Al_2O_3 = 17.09$, $H_2O = 12.5$ ($M_{H_2O} = 0.125$). Minerals included in the construction of the grid are garnet (grt), hornblende (hb), paragonite (pa), clinozoisite (cz), kyanite (ky), orthopyroxene (opx), clinopyroxene (cpx), and plagioclase (plag) with quartz in excess. The fluid phase is assumed to be pure H_2O. M_{H_2O} is defined as the molar proportion of the component, H_2O, in the bulk composition. A very narrow garnet–clinopyroxene-plagioclase quintivariant field (labelled) lies along the vertical axis at $M_{H_2O} = 0.0$. Divariant fields are filled light grey, trivariant fields are filled white and quadrivariant fields are filled dark grey. (b) Pseudosection in Fig. 7 contoured for THERMOCALC determined mineral modes (mole proportions normalised to one oxide). Dashed lines are mineral mode isopleths.

fluid. Figure 7(a) illustrates the change in assemblages from those at low-T involving a large change in assemblage with available amount of fluid, through assemblages involving mostly garnet and clinopyroxene at high temperatures.

The changes in mineralogy of the Mt Daniel rocks involved: (1) the consumption of garnet and clinopyroxene to form hornblende and clinozoisite; and (2) the consumption of hornblende and clinozoisite to form: (a) garnet and clinopyroxene; or (b) to form clinopyroxene–kyanite and clinozoisite–quartz–kyanite–plagioclase symplectites. Along the $M_{H_2O} = 0$ line there is an infinitely narrow anhydrous trivariant field that does not contain hornblende and the position of the garnet–clinopyroxene hornfels assemblage must lie within this infinitely narrow field. Estimates from garnet–clinopyroxene thermometry place the garnet–clinopyroxene hornfels assemblage at the top of the diagram but within the infinitely narrow garnet-plagioclase-clinopyroxene trivariant field. The development of the hornblende–clinozoisite assemblages must have involved the addition of H_2O to the rock and may be represented by a horizontal line on the pseudosection (Fig. 7a). Assemblages involving hornblende and clinozoisite are restricted to $T < 590$ °C and $M_{H_2O} > 0.06$ in the model system. A comparison of the observed modes of hornblende and clinozoisite (Table 1) with THERMOCALC determined modes (mole proportions normalised to one oxide) shown in Fig. 7(b), suggests that the hornblende–clinozoisite gneiss formed at approximately $T = 580$ °C and $M_{H_2O} = 0.1$ in the model system.

The near complete consumption of hornblende and clinozoisite in the cores of the garnet reaction zones is consistent with conditions at very low M_{H_2O}. The proportion of hornblende and clinozoisite decrease and the proportion of clinopyroxene and garnet increase as the core of the garnet reaction zone is approached, suggesting that the amount of dehydration increases toward the centre of the garnet reaction zones. Thus, the garnet reaction zone assemblage is unlikely to reflect the quadrivariant assemblage garnet–clinopyroxene-hornblende-plagioclase. The observed garnet and clinopyroxene modes place the garnet reaction zone assemblage at $M_{H_2O} \ll 0.01$ and $T =$ 575–590 °C in the model system (Fig. 7b). Such conditions involve lower temperatures than the thermobarometry presented above, by >100 °C. This is most probably due to inadequacies in the model system such as not modelling for Fe^{3+} as discussed further below. The symplectic intergrowths of clinopyroxene-kyanite and clinozoisite-quartz-kyanite-plagioclase adjacent to the garnet reaction zones also reflect lower water activity, although not as low as within the garnet reaction zones. The stability of kyanite in the symplectites constrains M_{H_2O} to the range 0.02–0.05 for $T = 575$–590 °C in the model system. The modal isopleths for hornblende, clinopyroxene and kyanite show similar slopes within the kyanite-bearing fields (Fig. 7b). This is consistent with the textural evidence that suggests S1 hornblende was replaced by symplectic intergrowths of clinopyroxene and kyanite.

The modelling does not take into account Fe^{3+} or Ti in any mineral. The lack of Fe^{3+} in the model is likely to have had a significant effect on the stability of clinozoisite on the diagram. We suggest that clinozoisite is stable at much higher temperature and lower M_{H_2O} than that shown on Fig. 7(a), if Fe^{3+} was considered. If this is correct, then the horizontal hydration and dehydration arrows on the pseudosection could be placed at higher temperatures than that shown. This would dramatically reduce the discrepancy between the temperatures estimated by the modelling and directly calibrated thermometry. Paragonite was not observed in the rocks at Mt Daniel and plagioclase was most commonly observed within the dehydration symplectites. However, paragonite and plagioclase appear in fields through which our interpreted T–M_{H_2O} path passes. We consider this is unimportant as the THERMOCALC model modes of paragonite and plagioclase reach a maximum of approximately 5% along the indicated path. The appearance of minor modal paragonite and plagioclase in the model may also be in part a function of using a bulk composition obtained from XRF, whereas the effective equilibration volume within which the symplectite reaction textures developed may have been slightly different. To test the sensitivity of the modelling to variation in bulk rock composition, we removed a small portion of Ca (tied up in titanite) and Fe (to account for some Fe^{3+}) from the bulk rock to see what effect this would have on the pseudosection (new bulk rock: $CaO = 30.43$, $Na_2O = 2.57$, $FeO = 20.26$, $MgO = 25.03$, $Al_2O_3 = 21.71$, $H_2O = 0.00$). We found that the topology of the pseudosection did not change. However, the boundaries between fields of different variance shifted up temperature by approximately 15–20 °C, suggesting that minor variations in the choice of bulk rock composition do not greatly influence the position of fields in the model system. To test if the effective equilibration volume within which the symplectite textures developed was different to the composition obtained via XRF, models for the bulk rock compositional ranges determined in Table 3 were also made. It was found that the mineral assemblages predicted for these bulk rock compositions did not match the observed assemblages particularly well. This supports the analysis of average bulk compositions (above and in Table 3) that suggests that the symplectite textures formed whilst there was chemical communication between the different textural domains in the rock.

CONCLUSIONS

Mafic granofels of the Arthur River Complex at Mt Daniel experienced hydration and dehydration at elevated temperatures in the mid- to deep-crust. Mafic hornfels were most probably produced by removal of

felsic material through the partial melting of more common Arthur River Complex dioritic to gabbroic bulk rock compositions, in response to emplacement of the Early Cretaceous Western Fiordland Orthogneiss batholith. However, it is possible that a more mafic variety of the Arthur River Complex was located at the Western Fiordland Orthogneiss contact at Mt Daniel. Regardless of the mechanism that developed the mafic rocks, the earliest metamorphic assemblages are preserved in pods of coarse-grained garnet–clinopyroxene hornfels. Hydration of the hornfels at 800–850 °C < T < 700–750 °C produced hornblende–clinozoisite mafic gneiss. The terrane was buried to deep crustal levels prior to the development of garnet reaction zones at $P \approx 12$ kbar and $T = 700$–750 °C. Limited dehydration adjacent to the garnet reaction zones promoted the development of symplectic intergrowths of clinopyroxene–kyanite and clinozoisite–quartz–kyanite–plagioclase.

ACKNOWLEDGEMENTS

Australian Postgraduate Awards supported NRD and JAS. Logistic and analytical expenses were met from Australian Research Council funding to KAK and GLC (A10009053) and National Science Foundation funding to KAK (EAR-0087323). We thank N. Mortimer and A. Tulloch of the IGNS, Dunedin for many helpful discussions and logistical assistance, and the Department of Land Conservation in Te Anau for permission to visit and sample localities in the Fiordland National Park. Thanks go to N. M. Kelly and A. Papadakis for their enthusiastic assistance in the field, to K. Stüwe and M. Hand for their critical reviews, and to R. Powell for his careful editing of the manuscript.

REFERENCES

Bence, A. E. & Albee, A. L., 1968. Empirical correction factors for the electron microanalysis of silicates and oxides. *Journal of Geology*, **76,** 382–403.

Bishop, D. G., Bradshaw, J. D. & Landis, C. A., 1985. Provisional terrain map of South Island, New Zealand. In: *Tectonostratigraphic Terranes of the Circum-Pacific Region* (eds Howell, D. G., Jones, D. L. Cox, A. & Nur, A.), pp. 512–522. Circum-Pacific Council for Energy and Resources, Houston.

Blattner, P., 1978. Geology of the crystalline basement between Milford Sound and the Hollyford Valley, New Zealand. *New Zealand Journal of Geology and Geophysics*, **21,** 33–47.

Blattner, P., 1991. The North Fiordland transcurrent convergence. *New Zealand Journal of Geology and Geophysics*, **34,** 553–542.

Bradshaw, J. Y., 1989. Origin and metamorphic history of an Early Cretaceous polybaric granulite terrain, Fiordland, southwest New Zealand. *Contributions to Mineralogy and Petrology*, **103,** 346–360.

Bradshaw, J. Y., 1990. Geology of crystalline rocks of northern Fiordland: details of the granulite facies Western Fiordland Orthogneiss and associated rock units. *New Zealand Journal of Geology and Geophysics*, **33,** 465–484.

Carson, C. J., Clarke, G. L. & Powell, R., 2000. Hydration of eclogite, Pam Peninsula, New Caledonia. *Journal of Metamorphic Geology*, **18,** 79–90.

Carson, C. J., Powell, R. & Clarke, G. L., 1999. Calculated mineral equilibria for the eclogite facies in Na_2O-CaO-FeO-MgO-Al_2O_3-SiO_2-H_2O: application to the Pouébo Terrane, Pam Peninsula, New Caledonia. *Journal of Metamorphic Geology*, **17,** 9–24.

Cawthorn, A. F. & Collerson, K. D., 1974. The recalculation of pyroxene endmember parameters and estimation of ferrous and ferric iron content from microprobe analyses. *American Mineralogist*, **59,** 1203–1208.

Clarke, G. L., Daczko, N. R. & Nockolds, C., 2001. A method for applying matrix corrections to X-ray intensity maps using the Bence-Albee algorithm and Matlab. *Journal of Metamorphic Geology*, **19,** 635–644.

Clarke, G. L., Klepeis, K. A. & Daczko, N. R., 2000. Cretaceous high-P granulites at Milford Sound, New Zealand: their metamorphic history and emplacement in a convergent margin setting. *Journal of Metamorphic Geology*, **18,** 359–374.

Clarke, G. L. & Powell, R., 1991. Decompressional coronas and symplectites in granulites of the Musgrave Complex, central Australia. *Journal of Metamorphic Geology*, **9,** 441–450.

Daczko, N. R., Clarke, G. L. & Klepeis, K. A., 2001. Transformation of two-pyroxene hornblende granulite to garnet granulite involving simultaneous melting and fracturing of the lower crust, Fiordland, New Zealand. *Journal of Metamorphic Geology*, **19,** 549–562.

Droop, G. T. R. & Bucher-Nurminen, K., 1984. Reaction textures and metamorphic evolution of sapphirine-bearing granulites from the Gruf Complex, Italian Central Alps. *Journal of Petrology*, **25,** 766–803.

Ellis, D. J. & Green, D. H., 1979. An experimental study of the effect of Ca upon garnet-clinopyroxene Fe-Mg exchange equilibria. *Contributions to Mineralogy and Petrology*, **71,** 13–22.

Ellis, D. J., Sheraton, J. W., England, R. N. & Dallwitch, W. B., 1980. Osumilite-sapphirine-quartz granulites from Enderby Land, Antarctica – mineral assemblages and reactions. *Contributions to Mineralogy and Petrology*, **72,** 353–367.

Guiraud, M., Powell, R. & Cottin, J.-Y., 1996. Hydration of orthopyroxene-cordierite-bearing assemblages at Laouni, Central Hoggar, Algeria. *Journal of Metamorphic Geology*, **14,** 467–476.

Hill, E. J., 1995a. The Anita Shear Zone: a major, middle Cretaceous tectonic boundary in northwestern Fiordland. *New Zealand Journal of Geology and Geophysics*, **38,** 93–103.

Hill, E. J., 1995b. A deep crustal shear zone exposed in western Fiordland, New Zealand. *Tectonics*, **14,** 1172–1181.

Kimbrough, D. L., Tulloch, A. J., Coombs, D. S., Landis, C. A., Johnston, M. R. & Mattinson, J. M., 1994. Uranium-lead zircon ages from the Median Tectonic Zone, New Zealand. *New Zealand Journal of Geology and Geophysics*, **37,** 393–419.

Kimbrough, D. L., Tulloch, A., Geary, E., Coombs, D. S. & Landis, C. A., 1993. Isotope ages from the Nelson region of South Island, New Zealand: structure and definition of the Median Tectonic Zone. *Tectonophysics*, **225,** 433–448.

Klepeis, K. A., Daczko, N. R. & Clarke, G. L., 1999. Kinematic vorticity and the tectonic significance of superposed mylonites in a major lower crustal shear zone, northern Fiordland, New Zealand. *Journal of Structural Geology*, **21,** 1385–1405.

Landis, C. A. & Coombs, D. S., 1967. Metamorphic belts and orogenesis in southern New Zealand. *Tectonophysics*, **4,** 501–518.

Leake, B. E., Woolley, A. R., Birch, W. D. *et al.*, 1997. Nomenclature of amphiboles. *Mineralogical Magazine*, **61,** 295–321.

Mattinson, J. L., Kimbrough, D. L. & Bradshaw, J. Y., 1986. Western Fiordland orthogneiss: Early Cretaceous arc

magmatism and granulite facies metamorphism, New Zealand. *Contributions to Mineralogy and Petrology*, **92,** 383–392.

Mortimer, N., Tulloch, A. J., Spark, R. N., Walker, N. W., Ladley, E., Allibone, A. & Kimbrough, D. L., 1999. Overview of the Median Batholith, New Zealand: a new interpretation of the geology of the Median Tectonic Zone and adjacent rocks. *Journal of African Earth Sciences*, **29,** 257–268.

Muir, R. J., Weaver, S. D., Bradshaw, J. D., Eby, G. N., Evans, J. A. & Ireland, T. R., 1996. Geochemistry of the Karamea Batholith, New Zealand, and comparisons with the Lachlan Fold Belt granites of SE Australia. *Lithos*, **39,** 1–20.

Newton, R. C. & Haselton, H. T., 1981. Thermodynamics of the garnet-plagioclase-Al_2SiO_5-quartz geobarometer. In: *Advances in Physical Geochemistry*, Vol. 1 (eds Newton, R. C., Navrotsky, A. & Woods, B. J.), pp. 131–147. Springer Verlag, New York.

Newton, R. C. & Perkins, D., 1982. Thermodynamic calibration of geobarometers based on the assemblages garnet-plagioclase-orthopyroxene-(clinopyroxene)-quartz. *American Mineralogist*, **67,** 203–222.

Powell, R., 1985. Regression diagnostics and robust regression in geothermometer/geobarometer calibration; the garnet-clinopyroxene geothermometer revisited. *Journal of Metamorphic Geology*, **3,** 231–243.

Powell, R., Holland, T. J. B. & Worley, B., 1998. Calculating phase diagrams with Thermocalc: methods and examples. *Journal of Metamorphic Geology*, **16,** 577–588.

Sandiford, M., Powell, R. & Neall, F., 1987. Metamorphic evolution of aluminous granulites from Labwor Hills, Uganda. *Contributions to Mineralogy and Petrology*, **95,** 217–225.

Wandres, A. M., Weaver, S. D., Shelley, D. & Bradshaw, J. D., 1998. Change from calc-alkaline to adakitic magmatism recorded in the Early Cretaceous Darran Complex, Fiordland, New Zealand. *New Zealand Journal of Geology and Geophysics*, **41,** 1–14.

Wood, B. L., 1972. Metamorphosed ultramafites and associated formations near Milford Sound, New Zealand. *New Zealand Journal of Geology and Geophysics*, **15,** 88–127.

Received 12 March 2001; revision accepted 23 March 2002.